Title: **A dynamic model combining the average and the local meshing stiffnesses and based on the static transmission error for spur gears with profile modification**

Authors: **M. Abruzzo, M. Beghini, C. Santus, F. Presicce**

DOI Link: https://doi.org/10.1016/j.mechmachtheory.2022.105139

A dynamic model combining the average and the local meshing stiffnesses and based on the static transmission error for spur gears with profile modification

M. Abruzzo[a,*], M. Beghini[a], C. Santus[a], F. Presicce[a]

[a]*DICI, Dipartimento di Ingegneria Civile e Industriale, University of Pisa, Italy.*

Abstract

A dynamic model that evaluates the working condition of general spur gears based on a two-phase approach is presented. A finite element model is preliminary developed to obtain the static transmission error for several angular configurations at different nominal torques. Subsequently, a lumped parameter model is used to evaluate the dynamic behavior of the transmission. An analytical mesh-force formulation is proposed based on polynomial interpolations of the finite element results to accurately model the contact forces and meshing stiffness during the engagement. Two damping models are implemented to obtain a reasonable estimation of the response peaks in resonance conditions. The stability of the main resonance peaks is examined using Poincaré maps. The results are compared with those obtainable using the commonly employed models based either on the average or the local meshing stiffness, highlighting the limitations of these approaches. The proposed formulation combines classical mesh stiffness definitions, thereby achieving a more accurate and efficient mesh-force model.

Keywords: Dynamic lumped parameter model; Finite element analysis; Nonlinear load and time varying meshing stiffness; Profile modifications; Spur gears.

*Corresponding author: Michele Abruzzo
Ph. +39 392 617 1705
Email address: michele.abruzzo@phd.unipi.it (M. Abruzzo)

Nomenclature

a	Center distance
b	Backlash
c_{m}	Meshing damping
d	Coefficient of dissipation
D_{f}	Dynamic factor
E_{dis}	Total dissipated energy
f_{m}	Meshing frequency
f_{r}	Natural frequency of the transmission
F_{m}	Meshing force
h	Profile modification
h_{a}	Addendum
h_{f}	Dedendum
h_{max}	Maximum profile modification
I	Rotational intertia of the gears
k_{a}	Average meshing stiffness
k_{l}	Local meshing stiffness
k_{m}	Meshing stiffness
K_{v}	Dynamic overload factor
L	Face width
m_{n}	Module
M_{T}	Static (or nominal) torque
n	Polynomial degree
q	Total relative mesh displacement
q_{in}	Initial relative mesh displacement
q_0	Static transmission error
q_{FEM}	Total relative mesh displacement of the finite element model
q_{rms}	Root mean square of the total relative mesh displacement
$\dot{q}_0$	Initial relative speed
$\dot{q}_{\mathrm{f}}$	Final relative speed
R_{b}	Base radius
R_{hub}	Hub radius
T	Period
v_{t}	Tangential speed of the gears
Z	Number of teeth
α	Pressure angle
η	Dynamic viscosity of the lubricant
λ	Curvilinear abscissa on the tooth profile
λ_0	Curvilinear abscissa on the tooth profile at the tooth tip
ϕ	Roll angle
ϕ_0	Gear angular step
ψ	Normalized roll angle
θ	Gear rotation angle
θ_0	Initial rotation
ζ	Damping ratio

1. Introduction

The increasing demand for high-performance transmissions characterized by a high transmitted power, especially in aeronautical applications, has led to the development of static and dynamic models that can accurately evaluate the system's working conditions. The need to distinguish between static and dynamic behaviors arises from the impossibility of neglecting the system's vibrations in predicting the durability and the maximum working loads of the transmission, especially in near-resonant conditions. This is particularly true for geared transmission systems, in which nonlinearities can cause self-induced vibrations [1].

Many of the models developed to analyze the dynamic behavior of gears are based on the transmission error, which quantifies the difference between the relative rotation of engaging gears considered as either ideally rigid or deformable bodies. Özgüven and Houser [1] reviewed the models developed until the 1990s, whereas Blankenship and Singh [2] studied how the meshing compliance could be included. Wang et al. [3] examined several nonlinear dynamic phenomena present in the vibration of gears, such as the effects of the varying contact ratio [4, 5] and of heavy loads [6]. Tamminana, Kaharaman and Vijayakar [7] studied how the static transmission error (i.e. the transmission error at very low speeds, when vibrations can be neglected) influences the dynamic loads experienced by the transmission at different powers and speeds. Other authors [8, 9] investigated theoretical aspects concerning the nonlinear dynamics of gears. Cai and Hayashi [10] proposed and experimentally validated an analytical model of the meshing compliance used for the development of lumped parameter models. The model was applied to spur gears without tooth profile modifications.

Several studies have demonstrated that tooth profile modifications can strongly influence the dynamic behavior of the gears. Kahraman and Blankenship examined the effect of the involute tip relief [11], Eritenel and Chen [12, 13] evaluated the effect of tooth surface microscopic features, such as surface roughness, and Sanchez et al. [14] considered the effect of tooth profile modifications both on the static and dynamic behavior of the transmission. The effects of profile shifts [15] have also been extensively studied.

The gear backlash can also affect the dynamic behavior of a transmission, especially in near-resonant conditions and for gears working at low torques and high speeds [16, 17, 18, 19]. In these conditions, the vibration amplitude can be so high that it produces total or partial contact loss between engaging teeth [20] and due to the backlash, this leads to intermittent contact, which abruptly changes the system's response [21].

Several models have been proposed to estimate the mechanical energy dissipation in gear transmissions due to the presence of non-conservative forces. These models take into account friction on the tooth flanks, windage and oil dispersion, friction on the supports of the shafts, dissipative properties of the gear materials [22] (such as thermo-elasticity), and the presence of, small and limited, plastic or viscous strains in the contact region [23]. Although in certain applications, the dissipation is minimized by design, its value is the most important parameter in near-resonant conditions because it defines the maximum dynamic overload experienced.

Bending-torsional coupling [24, 25] could also be important for the dynamics of some gear systems. If the displacement at the engaging teeth due to the compliance of the shafts and supports is comparable to that produced by the compliance of the meshing, neglecting the bending compliance could lead to an incorrect prediction of the dynamic behavior of the systems and, often, determines an underestimation of the dynamic overload. These considerations are also valid if applied to three-dimensional gear body natural modes [26].

Some studies have focused on the effects of manufacturing errors on the dynamics of gears. Velex and Mataar [27] studied the effect of shape deviations and gear mounting errors. Yang et al. [28] modeled tooth chipping, i.e. a piece of material breaking away from the tooth tip, and analyzed its influence on the dynamics of the transmission.

Several recent models for simulating the dynamic behavior of spur gears are based on a two-phase approach. Firstly, the static transmission error and the meshing stiffness are calculated by accurate static analyses based on finite element models or analytical models [29]. Subsequently, the dynamics of the system are studied using a lumped parameter model, characterized by high accuracy and high computational efficiency. However, the presence of a time-dependent and load-dependent meshing stiffness makes it challenging to set up an accurate dynamic model. Dai et al. [30] tried to overcome those difficulties using a hybrid method in which the meshing force is directly derived by introducing the force-displacement-angular configuration response surface, calculated

by a static finite element model. This approach gives adequate results but at the cost of a large number of static simulations needed to obtain an accurate representation of the response surface in a complete meshing cycle.

The present work proposes a general and computationally efficient hybrid method capable of modeling spur gears in static and dynamic conditions. An accurate finite element model is used to evaluate the static transmission error at different nominal torques and several angular positions during the engagement. The related surface response, which gives the meshing force for any nominal torque and configuration, was obtained by a combined interpolation technique based on polynomials and splines. In this way, the number of static simulations needed to obtain the required accuracy was reduced by one order of magnitude compared to other approaches in the literature. A torsional lumped parameter dynamic model based on the proposed meshing force formulation was then developed. The time and load-dependent equations of motion were integrated numerically, and different working conditions of the gears were simulated. The results were compared to those obtained by classic approaches (i.e., the average and the local meshing stiffnesses) and experimental results [31], demonstrating that both the average and the local meshing stiffness are required to obtain an accurate description of the dynamics of the system. Two damping models [32, 33] were used to estimate the dynamic overloads in the most dangerous working conditions and at different nominal loads.

2. Finite Element Model for static analysis

The static transmission error was calculated with an accurate 2-D finite element model. The parameters of the transmission, reported in Table 1 and represented in Fig. 1 (a), were taken from [34]. In the present application, a typical tip relief modification was included, which is often adopted in high-performance applications to reduce the vibration and noise of gear trains [35, 36]. The tip relief h (Fig. 1 (b)) was assumed to be a parabolic function of the curvilinear abscissa on the nominal involute tooth profile λ:

$$h(\lambda) = h_{\max}(\frac{\lambda}{\lambda_0})^2 \tag{1}$$

starting from the pitch point and reaching its maximum at the tooth tip ($h_{\max}$). Note that the proposed approach is general and any kind of tip relief function $h(\lambda)$ could be considered.

Parameter	Symbol	Value
Module	m_n	2 mm
Number of teeth	Z	50
Pressure angle	α	20°
Contact ratio	-	1.5
Base radius	R_b	47 mm
Addendum	h_a	2 mm
Dedendum	h_f	2.5 mm
Face width	L	20 mm
Center distance	a	100.5 mm
Hub radius	R_{hub}	10 mm
Backlash	b	0.5 mm
Rotational inertia of the gears	I	1526 kgmm^2
Maximum profile modification	$h_{\max}$	5μm

Table 1: Parameters of the transmission.

As shown in Fig. 1 (a), each gear body was modeled with five teeth. Considering that the theoretical contact ratio is equal to 1.5, a maximum of 2 teeth per gear is involved in a single meshing cycle, thus the total number of teeth modeled is sufficient to cover a complete meshing cycle. The end teeth, which are not involved in the contact, are unloaded and have a negligible influence on the static transmission error [37]. The contact between the engaging teeth was modeled with frictionless contact and target elements. One of the gears was fixed at its hub and the other was constrained by radial supports, thus reproducing an ideal hinge on its rigid shaft, and

loaded with a torque M_{T}. As is common in analyzing spur gears [37, 38], the finite element model was made up of four nodes quadrilateral generalized plane strain elements. The element size and distribution of the static finite element model adopted was based on [37], in which several parametric analyzes were used to quantify the influence of the various features of the finite element model parameters on the calculation of the gear meshing stiffness. Different element sizes were adopted for modeling the gear body, the teeth and the contact zone (Fig. 1 (a)). The thickness of the region with the minimum element size was chosen to be twenty times larger than the maximum theoretical Hertzian displacement produced at the maximum applied torque. The final element size was obtained after a convergence analysis based on the displacements at the gear hub. This was considered appropriate for accurately modeling all the main effects that could potentially influence the meshing dynamics, which are the compliance due to the Hertzian contact and the deformations of the tooth, the fillet region, and the gear body.

As the gear mounting shafts and their supports were considered to be ideally rigid, the total relative displacement in the direction of the line of contacts q was defined as $q = R_{\mathrm{b}1}\theta_1 + R_{\mathrm{b}2}\theta_2$, i.e. the algebraic sum of the displacements produced by the total rotation of each gear evaluated at its hub in two fixed Cartesian coordinate systems centered on each axis, θ_1 and θ_2 (Fig. 1 (a)). The static transmission error q_0 quantifies q when the gears operate at vanishing (or null) nominal angular speeds. As in the static finite element model, the first gear was fixed at its hub ($\theta_1 = 0$), $q_0 = q_{\mathrm{FEM}} = R_{\mathrm{b}2}\theta_2$.

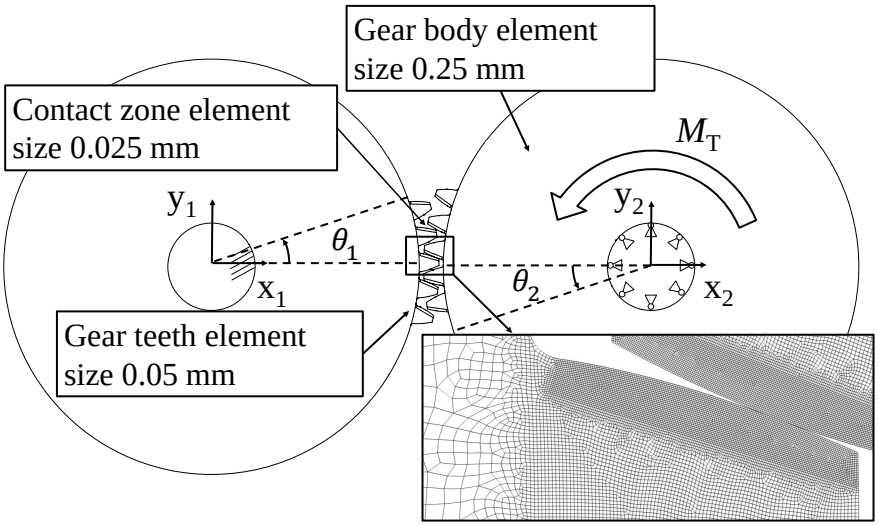

(a)

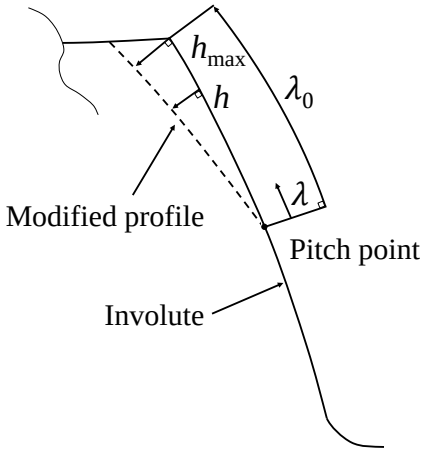

(b)

Figure 1: Static finite element model of the gears and profile modification. (a) Finite element model, detail of the element density, and definition of the gear body rotation angles θ_1 and θ_2 . (b) Detail of the tip relief (h is graphically magnified).

The finite element results were obtained with $M_T = [5; 10; 15; 30; 50; 80; 100; 150; 250]$ N m and at seventeen equidistant angular configurations covering the whole meshing cycle. Each configuration is defined by the roll angle ϕ, which is the angle whose arc on the base circle of radius unity equals the tangent of the pressure angle at a selected point on the involute, and the total angular step of the finite element model analysis is $\phi_0 = 2\pi/Z$.

In the general case, the number of M_T values should be sufficiently high to account for the nonlinearity of the meshing force, mainly close to the zero-load condition. Different load distributions (equally distributed or logarithmic) can be used for each case. In addition, the maximum torque considered should be at least three times higher than the nominal torque chosen for the dynamic analysis of the gear pair to avoid the extrapolation of the meshing force data during the dynamic analysis. The optimal number of angular configurations chosen depends on the smoothness of the static transmission error curves at any constant torque. Overall, at least fifteen to twenty points should be considered, and additional points can be added depending on the number of teeth, the maximum torque considered, and the profile modification (formulation and maximum value).

In Fig. 2, the finite element results for q_0 are plotted as a function of M_T and of the relative positions of the gears, defined as the normalized roll angle $\psi = \phi/\phi_0$. The static transmission error curves at constant M_T are similar for all the (non-zero) torques analyzed, and the transition from single tooth contact (STC) to double teeth contact (DTC) is regular. As expected, the peak to peak static transmission error increases with the torque. The main difference between the curves $q_0(\psi)$ for different M_T concerns the angular extension of the STC zone, which decreases when the torque is increased as an effect of the non-constant compliance during the meshing cycle.

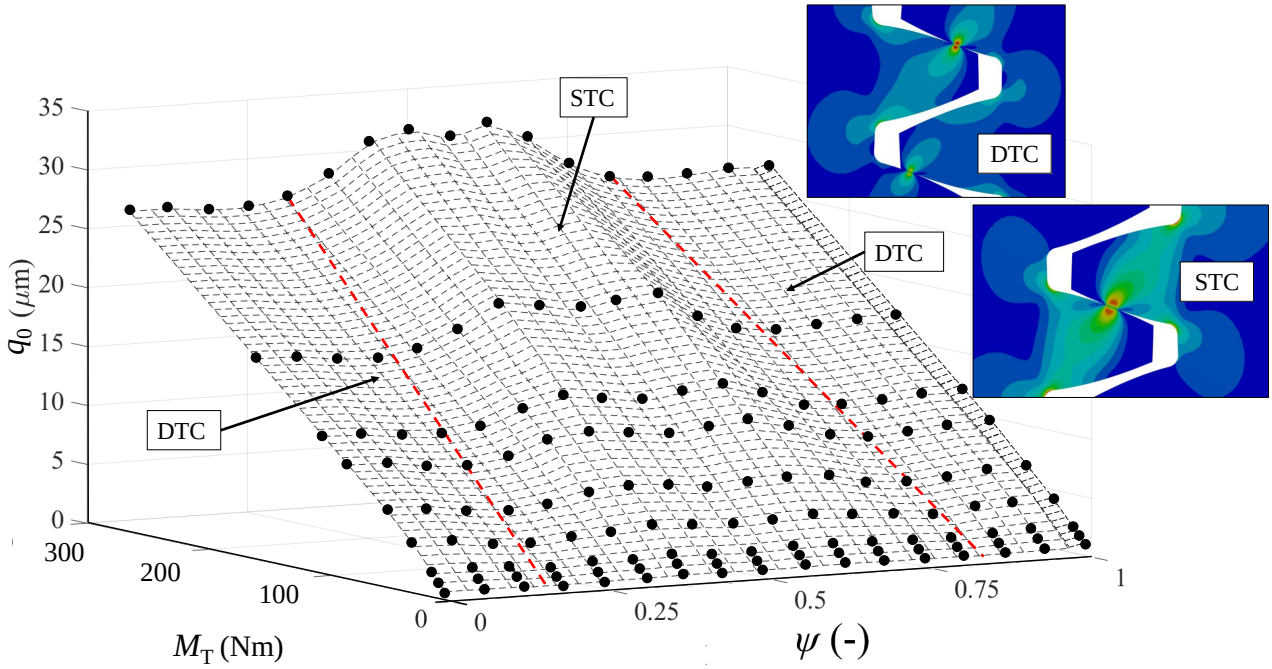

Figure 2: Static transmission error response surface obtained with the static finite element analysis. Regions where there is double teeth contact (DTC) and single tooth contact (STC) are highlighted.

3. Meshing stiffness definitions and response surface processing

The static transmission error can be used to calculate the meshing stiffness, which is the main parameter needed for the dynamic simulation of the system, and, in particular, for obtaining the current meshing force F_m. As the meshing force F_m is not proportional to the relative displacement q (see Fig. 3), in the literature two definitions of meshing stiffness are commonly adopted:

- The average, or secant, meshing stiffness k_a, defined as the ratio between the meshing force and the relative mesh displacement at a given configuration (k_a is the slope of the secant line OB in Fig. 3).
- The local, or tangent, meshing stiffness k_l, defined as the derivative of the meshing force with respect to the relative mesh displacement at a given configuration (k_l is the slope of the tangent line AB in Fig. 3).

The average and the local meshing stiffness can be directly used to build a meshing force model [29]. However, the nonlinear features of the contact between the gear teeth increase the meshing stiffness with the applied load (a stress-stiffening effect) which is needed to obtain an accurate dynamic model, as a single (even if variable) stiffness is not sufficient to characterize the meshing force at any time.

If only the average meshing stiffness is considered, a systematic underestimation of the meshing stiffness is produced, which only gives acceptable results for static analyses. The local meshing stiffness provides a more realistic value when modeling variations in relation to the nominal load, therefore it seems more suitable for predicting the effect of not-excessive vibrations. However, the local meshing stiffness can also generate inaccurate results when high dynamic overloads or contact loss phenomena are experienced by the transmission (i.e. in near-resonant conditions).

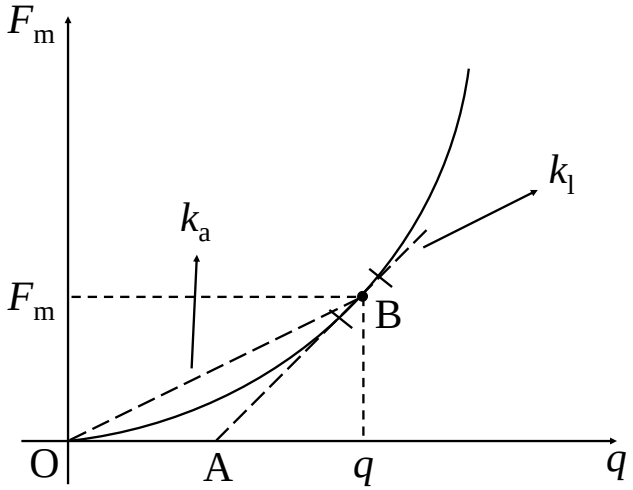

Figure 3: Meshing stiffness definitions and qualitative representation of the mesh-force relationship for a certain value of ψ.

To obtain the meshing stiffnesses, an analytical expression of the response surface of the meshing force was determined. In the most general case, the meshing force at each configuration ψ can be represented by an n-degree polynomial:

$$F_\mathrm{m}(q,\psi) = \sum_{j=1}^{n} a_j(\psi) q^j \tag{2}$$

where aj are coefficients that are obtained on the basis of the finite element results.
From eq. (1) the average and the local meshing stiffness can be calculated using their definitions:

$$k_\mathrm{a}(q,\psi) = \frac{F_\mathrm{m}(q,\psi)}{q} = \sum_{j=1}^{n} a_j(\psi) q^{j-1} \tag{3}$$

$$k_\mathrm{l}(q,\psi) = \frac{\mathrm{d}F_\mathrm{m}(q,\psi)}{\mathrm{d}q} = \sum_{j=1}^{n} j a_j(\psi) q^{j-1} \tag{4}$$

As shown in Fig. 4, in the example a parabolic interpolation of the meshing force ($n = 2$) produced an accurate fit of the response surface at all values of ψ. The determination coefficient between the forces calculated

with the least square parables and the values obtained by the finite element model was $r^2 = 0.998$ (Fig. 4b). The obtained coefficients a_j are reported in Appendix A.

For each position along the meshing cycle, k_a and k_l are linear functions of the relative displacement q. A linear spline interpolation in the ψ coordinate was used to evaluate the meshing force values in the regions between two adjacent simulated curves.

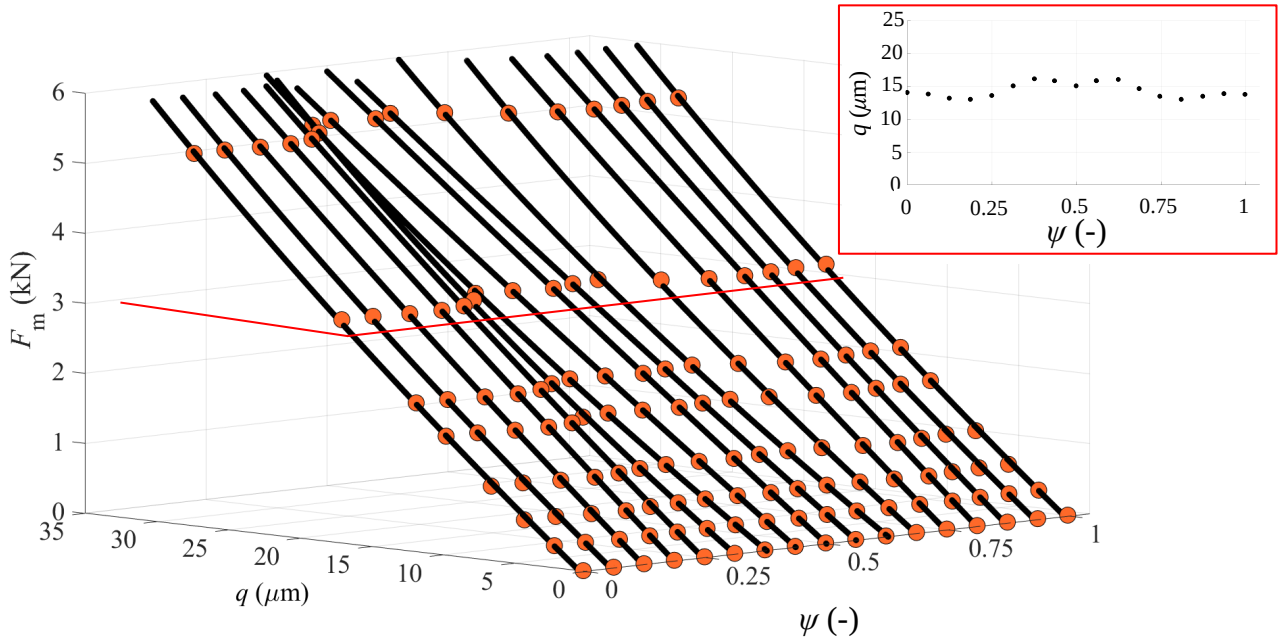

(a)

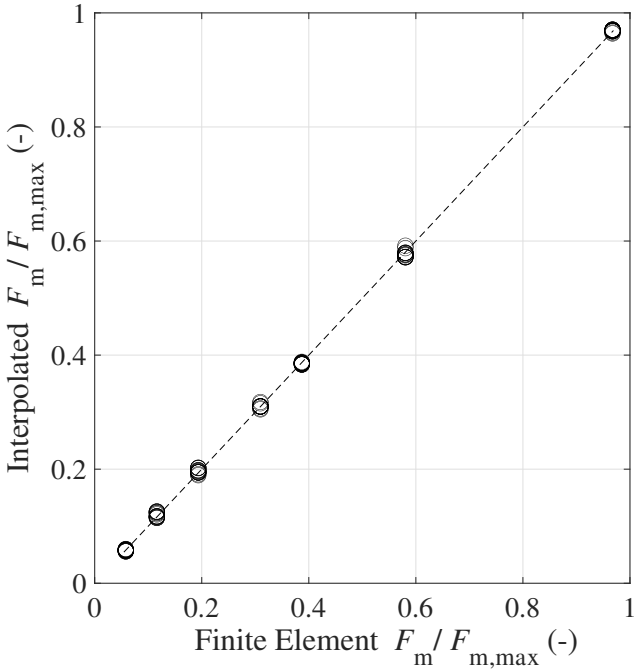

(b)

Figure 4: Response surface of the system. (a) Parabolic regressions of the force-displacement relationship in a single meshing cycle and contour plot for $F_m = 3$ kN. (b) Correlation diagram of the meshing force for all the examined conditions.

4. One degree of freedom dynamic model

As the lumped parameter model reproduces the engagement of two identical gears hinged at their hub, the only degrees of freedom were rotational. As shown in Fig. 5, the gears interact along the line of contacts (points A and B) through an equivalent nonlinear spring with a configuration dependent stiffness k_m in parallel with a damper c_m, introduced to include the energy dissipation. In addition, a backlash b was introduced to take into account possible contact loss on the active flanks and backside contact.

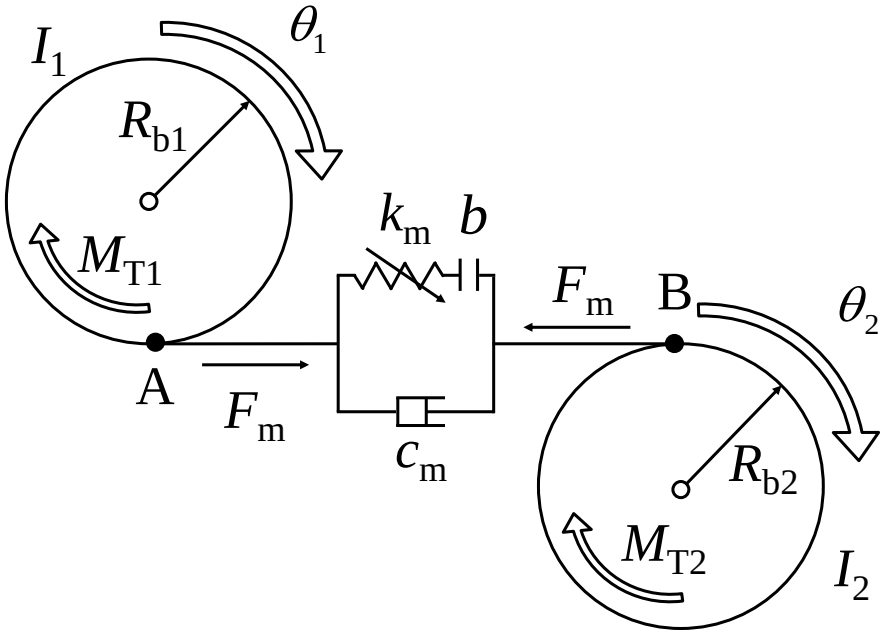

Figure 5: Lumped parameter model of the engaging gears.

In the most general form, if the lever arm of the meshing force variation due to the presence of a profile modification (usually small) is neglected, the equations of motion of the two gears can be written as:

$$\begin{cases} I_1\ddot{\theta}_1 + R_{b1}F_m = M_{T1} \\ I_2\ddot{\theta}_2 + R_{b2}F_m = M_{T2} \end{cases} \tag{5}$$

in which F_m is the total meshing force and M_{T1} and M_{T2} are the nominal torques applied at the hub of each gear. Considering the total relative displacement in the direction of the line of contacts q, the equation of motion can be rearranged into a single degree of freedom model:

$$m_e\ddot{q} + F_m = \frac{M_{T1}}{R_{b1}} = \frac{M_{T2}}{R_{b2}}, \quad m_e = \frac{I_1 I_2}{R_{b1}^2 I_2 + R_{b2}^2 I_1} \tag{6}$$

4.1. Model of the meshing force

In the dynamic model, at each time step i, k_a and k_l are calculated using the mesh displacement and the mesh force obtained at the previous time step $i-1$, and the numerical integration of the equation of motion is carried out considering the stiffness k_l. As anticipated, this approximation is valid for small variations of $q_i - q_{i-1}$, that is for small enough integration time steps. As a consequence, the current mesh force $F_{m,i}(q_i, \psi_i)$ is given by the sum of two contributions: the first is the mesh force at the previous step $F_{m,i-1}(q_{i-1}, \psi_{i-1})$, which is equal to $k_a(q_{i-1}, \psi_{i-1}) \cdot q_{i-1}$, and the increment is the mesh force variation, which depends on $k_l(q_{i-1}, \psi_i)$:

$$F_{m,i}(q_i, \psi_i) = k_a(q_{i-1}, \psi_{i-1}) \cdot q_{i-1} + k_l(q_{i-1}, \psi_i) \cdot (q_i - q_{i-1}) \tag{7}$$

An example of the mesh force calculation procedure is reported in Fig.6.

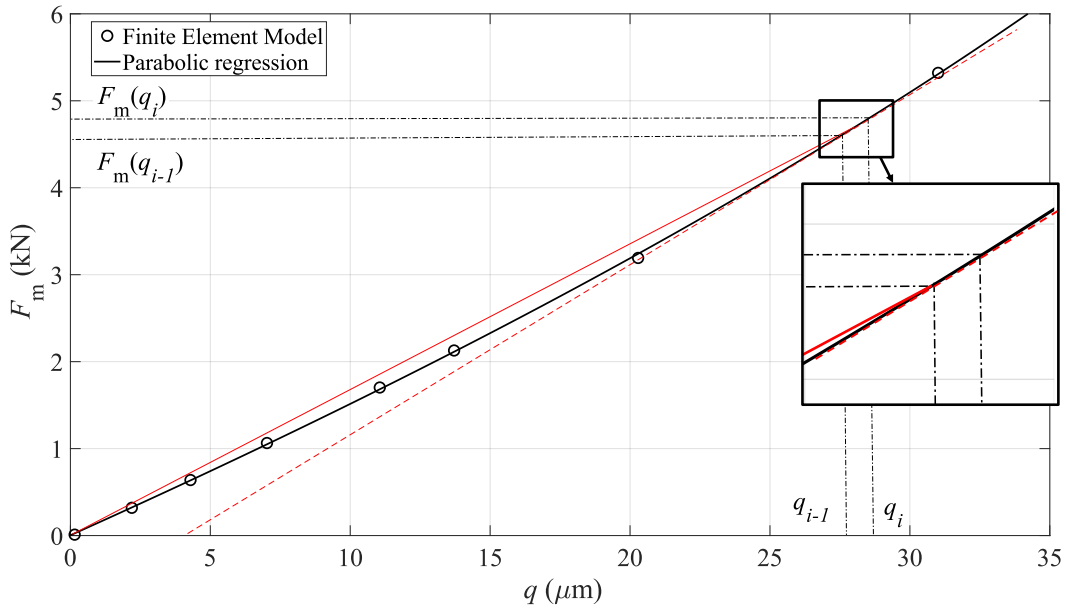

Figure 6: Mesh force calculation procedure at $\psi = 0.3$

By including the energy dissipation and the backlash between the gear teeth b, the current value of the meshing force is given by the following expression:

$$F_{m,i}(q_i,\psi_i) = \begin{cases} c_m\dot{q}_i + k_a(q_{i-1},\psi_{i-1})\cdot q_{i-1} + k_l(q_{i-1},\psi_i)\cdot(q_i - q_{i-1}) & \text{for} \quad q_i > 0 \\ 0 \quad \text{for} \quad q_i \le 0 \\ c_m\dot{q}_i + k_a(q_{i-1}+b,\psi_{i-1})\cdot(q_{i-1}+b) + k_l(q_{i-1}+b,\psi_i)\cdot(q_i - q_{i-1}) & \text{for} \quad q_i \le -b \end{cases} \tag{8}$$

The energy dissipation is modeled using the results of [32] and Gerber's semi-empirical damping model [33], whose details are reported in Appendix B. The first model gives the damping ratio ζ based on the energy dissipated only for the impact of the gears. This model provides an underestimation of the dissipation. Gerber's model is based on an empirical formula obtained by the values of the energy dissipation, and can be considered a typical value of the damping ratio ζ accounting for several dissipative effects active in gears. For both models, the damping coefficient c_m is calculated as:

$$c_m = \zeta \frac{2\pi f_r I}{R_{b^2}} \tag{9}$$

in which f_r is the natural frequency of the transmission.

4.2. Integration algorithm

The dynamic response of the gear pair is obtained by direct time integration of the equation of motion (5) relative speed and load/configuration dependent parameters. The algorithm (Fig. 7) is used to simulate two working conditions:

- Steady-state. The torque and the rotational speed of the system are kept constant and several steady-state load conditions are examined.
- Steady-state speed ramps. The rotational speed of the gears is either increased (Ramp-Up or RU) or decreased (Ramp-Down or RD) under constant M_T using speed steps of 50 rpm and enabling the system to reach steady-state conditions at each step.

Following Shampine and Reichelt [39], a numerical study of the integration scheme was carried out in order to ensure accurate results. The ODE113 (Adams-Bashfort-Moulton) with a maximum relative integration tolerance of 10^{-6} was used to characterize the dynamic behavior of the system.

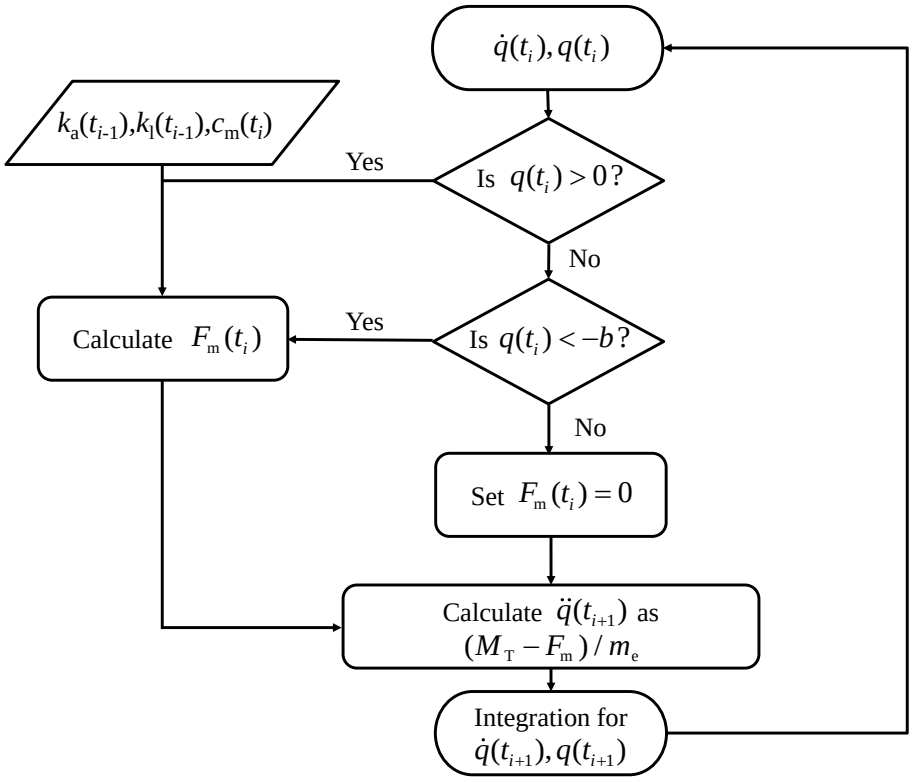

Figure 7: Integration algorithm.

5. Numerical results

The dynamic response of the system is investigated considering a meshing frequency f_m, the product of the rotational frequency of the gears and the number of teeth, up to 5 kHz (1.5 kHz above the natural frequency of the transmission). The envelope of the maximum and the minimum values of the dynamic factor D_f, defined as the ratio between the maximum and the minimum meshing force and its nominal value, is considered the most significant parameter of the dynamic analysis for two reasons: the maximum value of D_f represents the dynamic overload, usually indicated as K_v, and the minimum value of D_f is used to detect the contact loss phenomena when it is equal to 0.

Many parameters characterize the system and considering every combination would lead to an infinite number of analyses. For this reason, the most significant comparisons and results are reported in the following subsections. The dynamic response of the system is investigated during stepped ramp-up and stepped ramp-down. Then, the effect of the damping on the dynamic behavior of the system is studied to highlight any bifurcation due to the non-linearity and the influence of damping on the results obtained. The effect of the nominal torque is also studied, highlighting frequency shifts and changes in the response peaks of the system. The dynamic responses of the gear pair with and without profile modifications are compared. Finally, an example is shown of spectral and stability analyses of the most intense resonance peaks of the transmission.

5.1. Results of the proposed model during steady-state speed ramps

The dynamics of the gears obtained with the proposed approach during stepped ramp-up (RU) and stepped ramp-down (RD) are reported in Fig. 8. As a reference condition, the minimal damping and a nominal torque of 50 N m are considered. The resonance peak matching the natural frequency of the system is found at 3.4 kHz (point 4). In this condition a K_v of 3 is found. All the other resonance peaks can be attributed to super-harmonics of the meshing frequency (2x, 3x, 4x). No back-side contact is detected in the frequency range analyzed, but contact loss is predicted at 1.7 and 3.4 kHz (points 3 and 4). Jump phenomena are present at each resonance peak. They are a typical feature of nonlinear systems in which the vibration amplitude drops suddenly at a certain

frequency. A bifurcation in the behavior of the system can be observed in relation to the different type of speed ramp considered. During ramp-down (from 5 kHz), the transmission experiences a dynamic overload higher than the one experienced during ramp-up, with a 20% increase in the K_v at 1.7 kHz (point 3). The resonance peaks and the regions where there is contact loss are also wider (points 3 and 4).

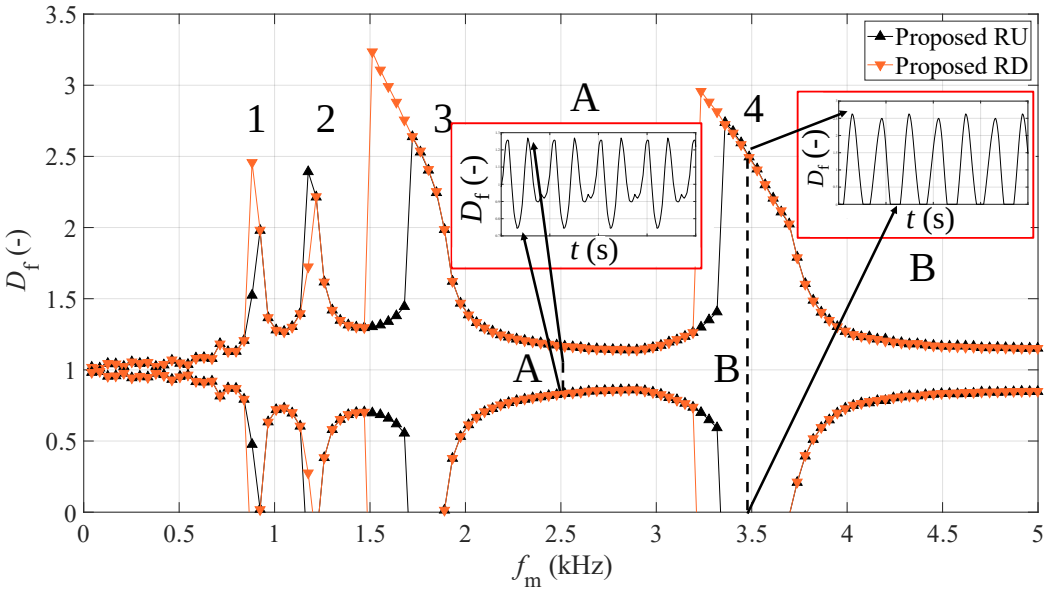

Figure 8: Dynamic factor during ramp-up and ramp-down considering the minimal damping and $M_T = 50$ N m with representation of the dynamic factor envelope at two different meshing frequencies, with (B) and without (A) contact loss.

5.2. *Comparison between damping models*

The effect of damping is shown for $M_T = 50$ N m in Fig. 9. The resonance peaks are found at the same frequencies (difference less than 0.3 kHz). If Gerber's model is adopted, there is no jump, and the resonance peaks are smoother and less intense ($K_v < 2.5$). Moreover, contact loss is predicted only at 1.7 kHz (point 3), and no bifurcation in the behavior of the system is detected in the whole frequency range of interest.

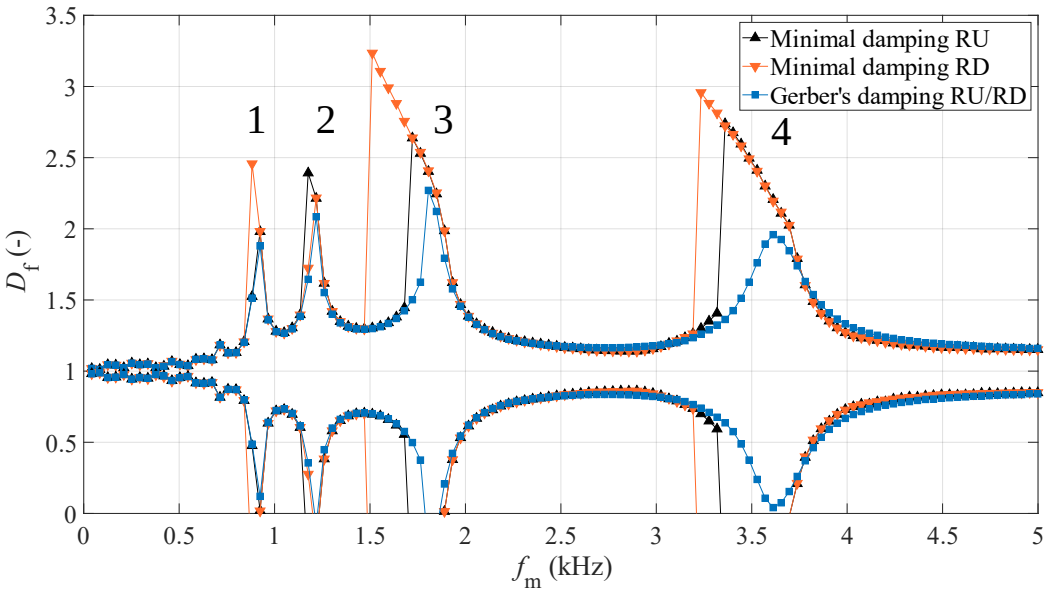

Figure 9: Comparison between the lower bound damping and Gerber's damping model.

5.3. *Effect of the nominal torque*

The analysis at different values of M_T highlights the nonlinear features of the system due to the load-varying stiffness (Fig. 10). At higher nominal torques, more resonance peaks at lower frequencies can be observed (below point 1), together with contact loss at 3.4 kHz for M_T >50 N m (point 4). Increasing the nominal torque at M_T >10 N m reduces the dynamic overload at 0.85 and 1.7 kHz (points 2 and 3), while the dynamic overload at 3.4 kHz increases (point 4). All the resonance peaks of the system are shifted at higher frequencies as the load increases. For reasons of clarity, the results are reported only with Gerber's damping model since its usage makes the visualization of the frequency shifts easier.

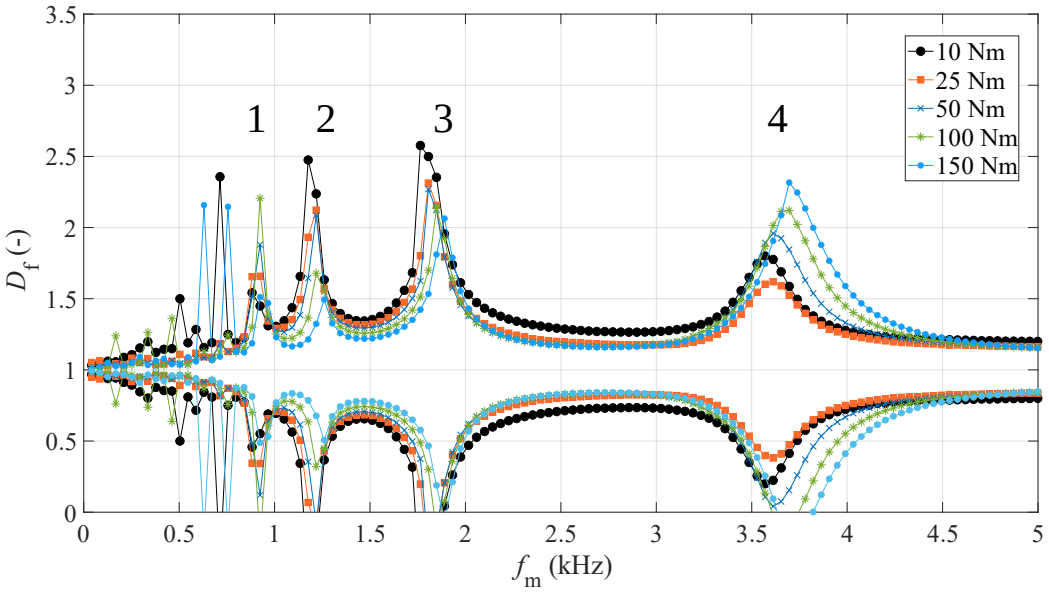

Figure 10: Comparison between the dynamic factor obtained with Gerber's damping model at different values of M_T.

5.4. *Comparison between gears with and without profile modifications*

The dynamic responses of the gears with and without profile modifications were compared using Gerber's model and a nominal torque M_T =50 N m (Fig. 11). Overall, the resonance peaks are at the same meshing frequencies (maximum relative difference of 10% at point 4). The most significant difference is in the intensity of the resonance peaks. For the gears without profile modifications, the resonance peak at 3.4 kHz (point 4) is more intense and wider. In addition, the resonance peaks due to the super-harmonics of the meshing frequency (points 1, 2, and 3) are less intense compared to the gear pair with a parabolic profile modification (for which contact loss is also present).

5.5. *Spectral and stability analysis of the main resonance peaks*

The spectral content of the total mesh displacement at $M_T = 50$ N m and considering the minimum damping is shown at the meshing frequencies of 1.7 kHz and 3.4 kHz (points 3 and 4) in Fig. 12. In both cases, the oscillation frequency is equal to the natural frequency of the transmission, however the harmonic contribution changes. The harmonics of interest are the meshing harmonic and its 2x and 4x super-harmonics, which cause the resonance peak at 3.4, 1.7, and 0.85 kHz, respectively (points 4, 3 and 2). In additions, given the high energy content of the first and the second harmonics, the resonance peaks experienced at 3.4 kHz and 1.7 kHz (points 4 and 3) are more intense than the others.

The stability of the steady-state response of the gears at the main resonance peaks (1.7 and 3.4 kHz) is investigated using Poincaré maps, representing the time evolution of the system's trajectories, in which an initial relative displacement q_{in} is imposed on the gears. The maps are obtained considering different values of q_{in} and different damping ratios ζ. As shown in Figs. 13 and 14, after a certain number of meshing cycles the trajectories

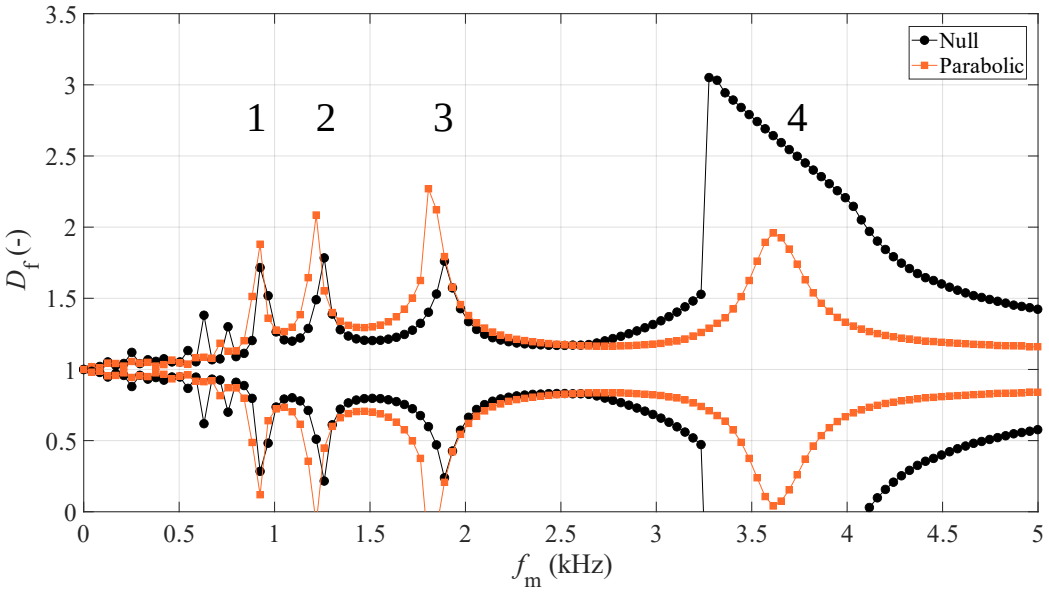

Figure 11: Comparison between the dynamic factor obtained for gears with and without profile modifications with Gerber's damping model and $M_T = 50$ N m.

of the system converge to a stable motion (when the relative difference between the maximum value of the mesh displacement between one meshing cycle and the next is less than 0.1%) regardless of the initial displacement imposed or the damping ratio. The only difference between the curves concerns the maximum displacement experienced during the initial transient motion and the time needed for the system to reach stable conditions, which are reduced if ζ is increased or q_{in} reduced. It can be concluded that at the main resonance frequencies, the system is stable.

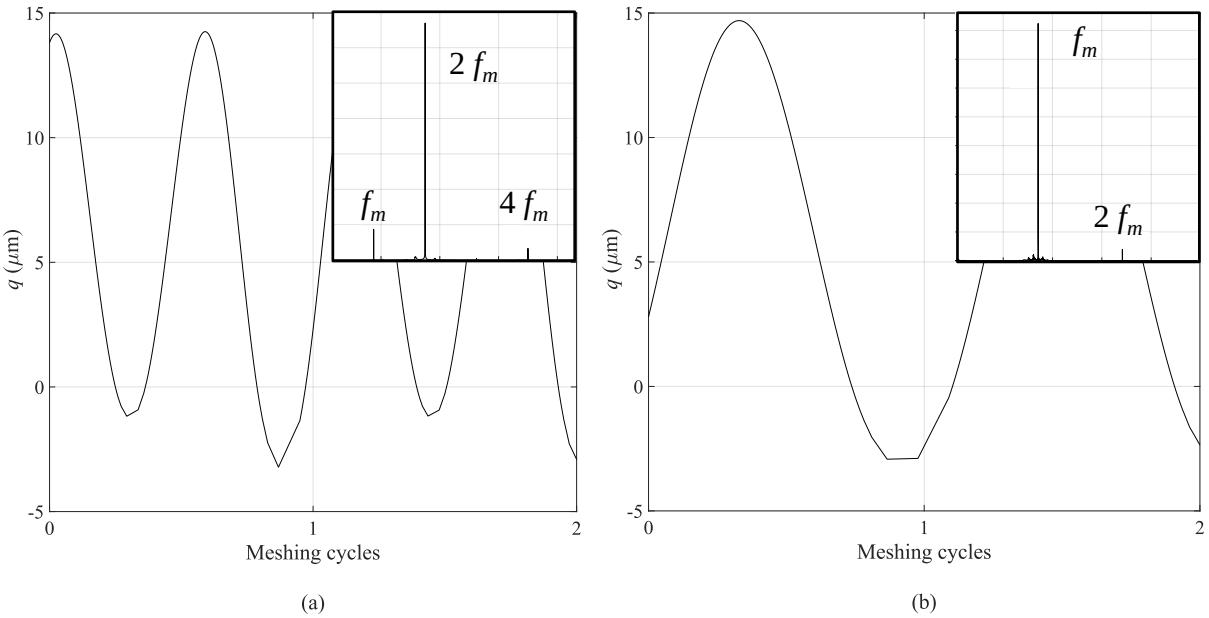

Figure 12: Spectral content of the total mesh displacement at the main resonance peaks. (a) $f_m = 1.7$ kHz. (b) $f_m = 3.4$ kHz.

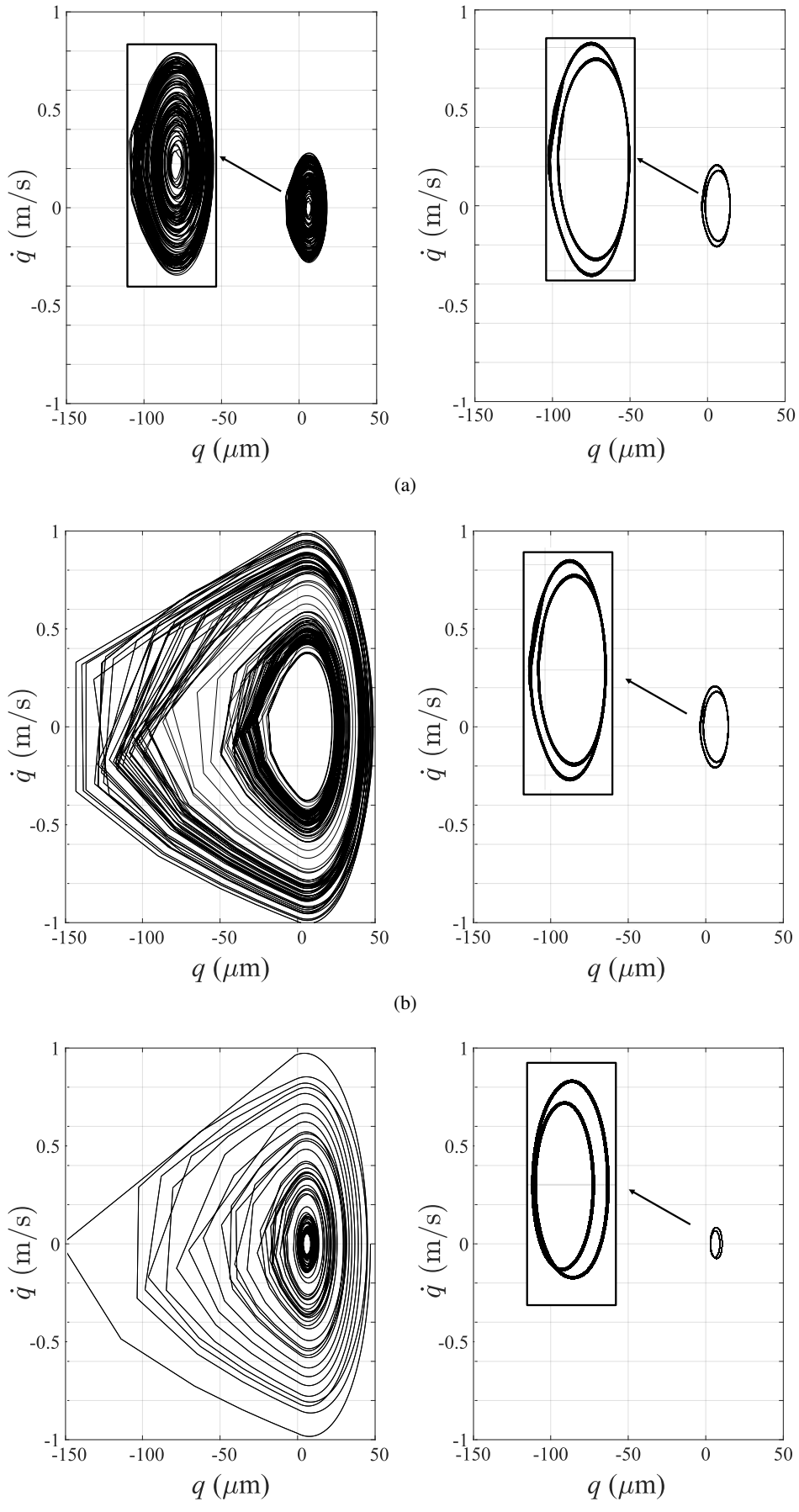

Figure 13: Poincaré maps obtained at 1.7 kHz and at different values of θ_0 and ζ. First and last 100 meshing cycles at (a) $\theta_0 = 0.00005$ and $\zeta = 0.001$, (b) $\theta_0 = 0.0005$ and $\zeta = 0.001$, (c) $\theta_0 = 0.00005$ and $\zeta = 0.01$. The number of meshing cycles required to reach convergence is 430, and the total number of simulated meshing cycles is 5000.

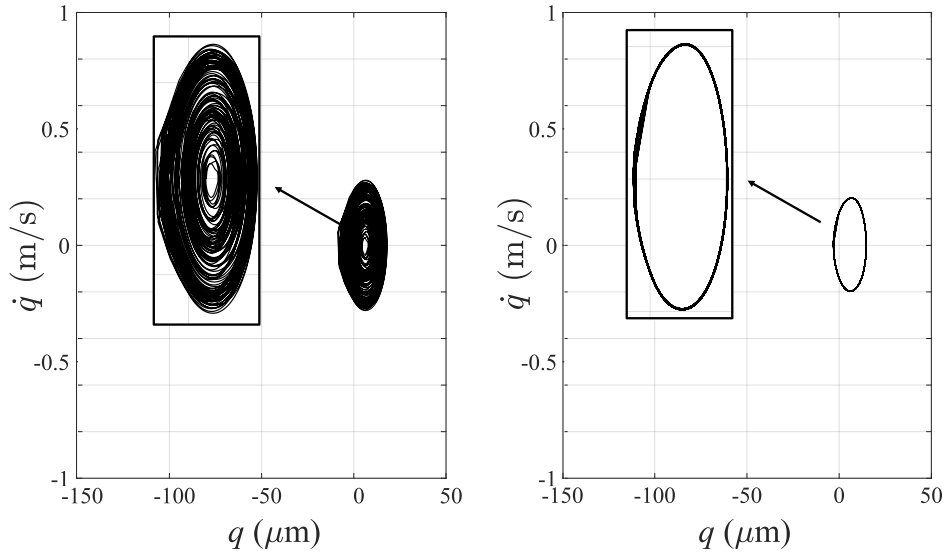

(a)

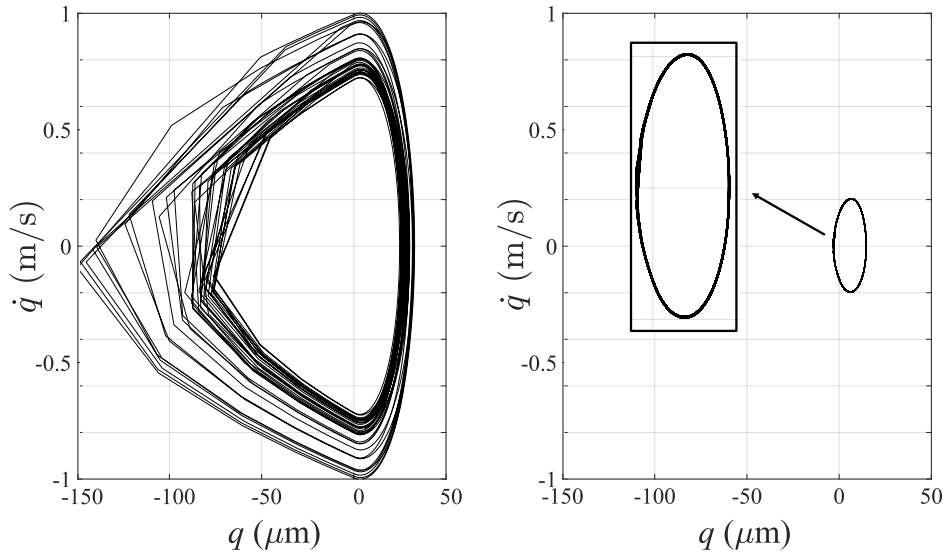

(b)

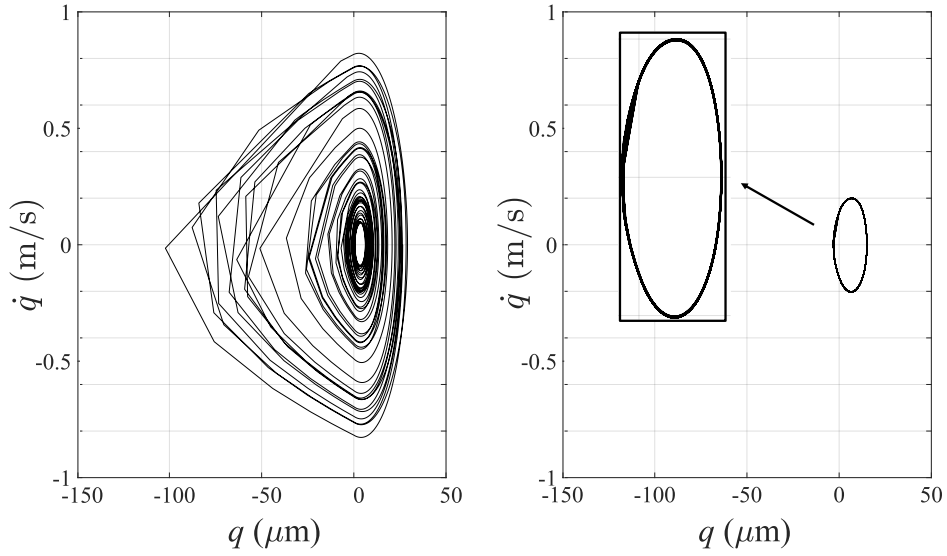

(c)

Figure 14: Poincaré maps obtained at 3.4 kHz and at different values of θ_0 and ζ. First and last 100 meshing cycles at (a) $\theta_0 = 0.00005$ and $\zeta = 0.001$, (b) $\theta_0 = 0.0005$ and $\zeta = 0.001$, (c) $\theta_0 = 0.00005$ and $\zeta = 0.01$. The number of meshing cycles required to reach convergence is 1350, and the total number of simulated meshing cycles is 5000.

6. Validation with experimental results

In this section, the proposed model is applied to a different gear pair. The dynamic results obtained with the proposed model were compared with the experimental data derived from the literature and the average and the local meshing stiffness models.

6.1. Static transmission error calculation

The transmission parameters were taken from Hotait and Kahraman [31] and are reported in Table 2. In the example, there has been no modification to the profile, but the outer diameter is smaller than the standard design value, thus reducing the theoretical contact ratio from 1.8 to 1.37.

Parameter	Symbol	Value
Module	m_n	3 mm
Number of teeth	Z	50
Pressure angle	α	20°
Contact ratio	-	1.37
Base radius	R_b	70.48 mm
Addendum	h_a	1.87 mm
Dedendum	h_f	3.75 mm
Face width	L	20 mm
Center distance	a	150 mm
Hub radius	R_{hub}	25 mm
Backlash	b	0.5 mm
Rotational inertia of the gears	I	12846 kgmm^2

Table 2: Parameters of the transmission.

The static transmission error was calculated during a complete meshing cycle using the same finite element model considerations reported in Section 2. The torque used for the comparison was 200 N m, and the static transmission error curves were obtained accordingly. The finite element results were obtained with $M_T = [15; 30; 50; 80; 100; 150; 200; 250; 300; 400; 500; 600]$ N m and at forty equally spaced angular configurations covering the entire meshing cycle. In this case, a higher number of angular configurations is required in order to accurately model the transmission error curves, especially to locate the maximum static transmission error point in the transition from the single tooth contact zone to the double tooth contact zone.

In Fig. 15, the finite element results for q_0 are plotted as a function of M_T and the relative positions of the gears ψ. As with the previous gear pair (Section 2), the static transmission error curves at constant M_T are similar for all the (non-zero) torques analyzed, and the transition from single tooth contact (STC) to double teeth contact (DTC) is regular. As expected, the peak-to-peak static transmission error increases with the torque, and the STC zone decreases when the torque is increased as an effect of the non-constant compliance during the meshing cycle.

6.2. Dynamic results

As in the experimental study, the dynamic response of the system was investigated considering a meshing frequency f_m up to 3.5 kHz, and the output of the dynamic analysis is the root mean square of the oscillating component of the total relative mesh displacement q_{rms}.

Figure 16 compares the results obtained by the proposed method with the experimental data and with the results that can be obtained if the analyses are conducted using either the average meshing stiffness k_a or the local meshing stiffness k_l. In the comparison, a constant damping ratio $\zeta = 0.01$ and a nominal torque of 200 N m were considered. In the experimental results, there are at least five different resonance peaks (points 1 to 5 in Figure 16), and all of them were correctly predicted by the three mesh force models. The only difference is in the amplitude of the low-frequency peaks (points 1, 2, and 3), suggesting that different damping values should be considered for a more accurate prediction of the experimental results.

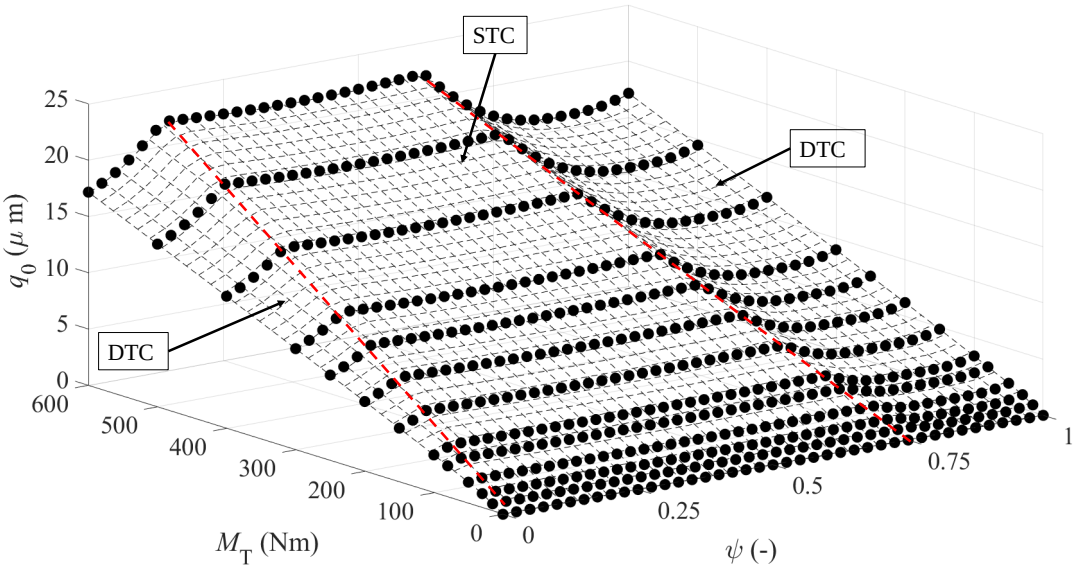

Figure 15: Static transmission error response surface obtained with the static finite element analysis. Regions where there is double teeth contact (DTC) and single tooth contact (STC) are highlighted.

The model with k_a shows a good agreement with the experimental results during stepped ramp-up (RU) simulations. However, the resonance peaks predicted are wider, and the dynamic overload experienced at 0.7, 1.35, and 2.7 kHz is overestimated (points 2, 4, and 5). Jump phenomena (points 4 and 5) are predicted at lower frequencies, and this causes a slight overestimation of q_{rms} outside the resonance condition.

The model based on k_l better estimates the resonance frequency and produces a more accurate result far from resonant conditions. However, in near-resonant conditions, the local stiffness causes a systematic underestimation of the meshing stiffness, and back-side contact is present. At 1.35 and 2.7 kHz (points 4, and 5), the system is unstable, consequently no corresponding points are reported in Fig. 16. The local stiffness calculated at the nominal meshing force is not suitable for studying the behavior of the system when high dynamic overloads are expected.

Our method shows the best agreement with the experimental results because it retains the main features of the previously discussed methods. q_{rms} is accurately estimated at any meshing frequency, showing a similar trend to the one obtained with k_a in resonance conditions and similar to the one obtained with k_l outside resonant conditions. In addition, our method is the only one that can predict the bifurcation phenomena shown in the experimental data at 1.35 and 2.7 kHz (points 4 and 5), obtaining an accurate estimation of the resonance frequency and q_{rms} even during stepped ramp-down (RD). The results obtained with the local and the average meshing stiffness show no bifurcation since the load nonlinearities are not considered. In conclusion, considering a nonlinear formulation accounting for the meshing stiffness variations due to the instantaneous load is fundamental when predicting possible bifurcations.

7. Conclusions

A one degree of freedom dynamic model for a gear transmission system based on a novel meshing stiffness formulation is presented. A finite element analysis, which can be used to account for any tip relief, was used to obtain the static transmission errors at different angular configurations and nominal torques. The static transmission error curves were interpolated at each position considered along the meshing cycle using a series of polynomial regressions and linear splines to take into account the stress stiffening properties of the contact and reducing the number of preliminary static simulations required. The required stiffnesses were calculated as a function of the instantaneous load applied, obtaining a more accurate representation of the behavior of the transmission (either in static or dynamic conditions).

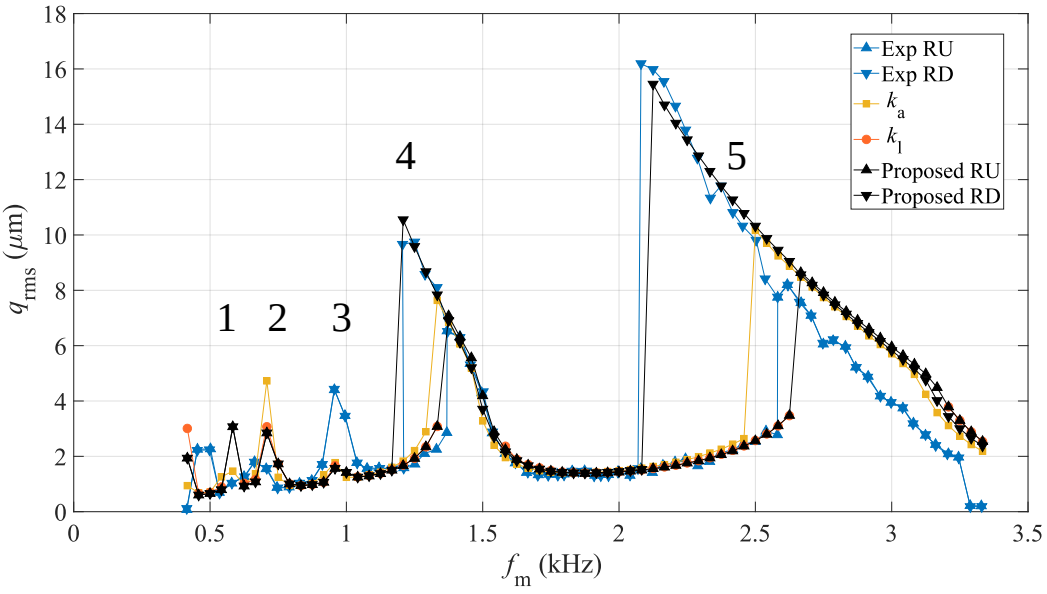

Figure 16: Comparison between meshing force formulations and experimental data considering $\zeta = 0.01$ and $M_T = 200$ N m.

Based on the novel contact formulation proposed, a lumped parameter model was developed. A simulation of the transmission was then obtained as a function of the meshing frequency, at different nominal torques, in steady-state conditions at different meshing frequencies, and in steady-state speed ramps.

The main resonance peaks of the system were obtained with two damping models, analyzing how the level of energy dissipation can affect the behavior of the transmission. The simulations at different nominal torques were used to highlight frequency shifts and how the stress-stiffening properties of the contact can change the system's dynamic response. The effects of angular accelerations and decelerations, which lead to the bifurcation in the behavior of the system, were also examined. In particular, a notable difference was observed between the ramp-up and the ramp-down steady-state speed ramps in the intensity of the predicted resonance peaks and in their frequency extension. We have proposed a dynamic analysis of the same gear pair with and without profile modifications. The spectral content of the most intense resonance peaks of the system was characterized, and the stability of the system was studied using Poincaré maps.

The proposed model was also used to study a second gear pair for which the dynamic behavior of the transmission was already experimentally available. The results were compared with the experimental data and with the output curves obtained using classical methods, i.e. the average meshing stiffness and the local meshing stiffness. The comparison highlights that there are few differences between the three models and that there is a good agreement with respect to the experimental data during stepped ramp-up simulations. Despite this, our method was the only one able to predict the ramp-up vs. ramp-down bifurcations.

Compared to the classic methods, the combination of the average and the local meshing stiffness retains the advantages of each mesh-force formulation, avoiding numerical instabilities (such as the ones present using the local meshing stiffness). The combined formulation shows a better agreement with experimental data, especially when highly nonlinear phenomena are present. Moreover, including the load dependency of the combined meshing stiffness allowed to obtain accurate results even during the ramp-down simulation when bifurcation phenomena are experienced.

The proposed approach is general and numerically efficient, and different profile modifications can be considered for static and dynamic analyses. Therefore, these results could be used for the optimal design of gear profile modifications also accounting for the dynamic behavior of the transmission.

Appendix A. Regression coefficients of the response surface

Appendix A.1. Gears with parabolic profile modification

As shown in Section 3, a parabolic formulation of the meshing force ($n = 2$) produces an accurate representation of the response surface of the system at any value of ψ considered in the finite element simulation. Table 2 shows the coefficients a_j for all the angular configurations considered.

ψ	a_1 (MN/m)	a_2 (GN/m^2)
0	173.4	882.7
0.06	174.5	829.5
0.13	184.9	511.4
0.19	192.3	240.9
0.25	183.4	449.2
0.31	155.1	1032.8
0.38	141.1	882.5
0.44	156.7	209.7
0.5	164.1	150.4
0.56	156.7	209.7
0.63	141.1	882.5
0.69	155.1	1032.8
0.75	183.4	449.2
0.81	192.3	240.9
0.88	184.9	511.4
0.94	174.5	829.5
1	173.4	882.7

Table 3: Regression coefficients.

The coefficients a_j are normalized with their maximum values and are represented as a function of ψ in Fig. A.17.

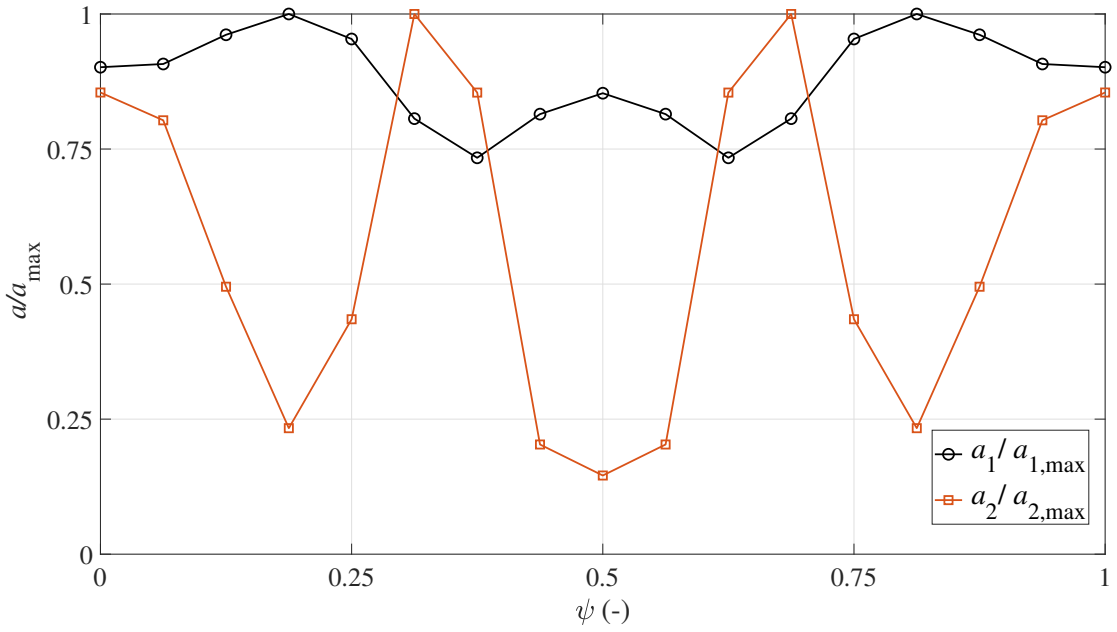

Figure A.17: Regression coefficients normalized with their maximum values in a single meshing cycle.

Appendix A.2. Gears without profile modification

For the gears from [31], a cubic formulation of the meshing force ($n = 3$) was needed to produce an accurate representation of the response surface of the system at any value of ψ considered in the finite element simulation. Table 4 shows the coefficients a_j for all the angular configurations considered.

ψ	a_1 (MN/m)	a_2 (TN/m^2)	a_3 (PN/m^3)
0	380.0	14.3	-441.6
0.025	316.7	18.7	-536.4
0.05	298.4	14.8	-325.4
0.075	326.1	5.3	34.2
0.1	360.9	-1.1	190.9
0.125	366.2	-0.6	84.6
0.15	353.2	2.4	-47.5
0.175	355.1	2.4	-45.3
0.2	355.8	2.4	-47.6
0.225	356.7	2.5	-48.8
0.25	357.4	2.5	-49.1
0.275	358.2	2.5	-49.1
0.3	358.8	2.5	-48.6
0.325	359.1	2.5	-49.5
0.35	359.4	2.5	-49.1
0.375	359.5	2.5	-49.5
0.4	359.4	2.5	-49.2
0.425	359.3	2.5	-49.0
0.45	358.9	2.5	-49.0
0.475	358.3	2.5	-49.2
0.5	357.7	2.5	-48.5
0.525	356.7	2.5	-49.3
0.55	355.8	2.5	-48.9
0.575	354.8	2.4	-47.7
0.6	353.8	2.4	-46.5
0.625	357.1	1.4	-2.7
0.65	370.0	-2.4	206.3
0.675	342.9	1.5	157.2
0.7	304.9	11.1	-164.4
0.725	300.7	18.2	-480.7
0.75	345.8	17.5	-529.2
0.775	415.0	11.1	-344.9
0.8	469.6	5.1	-145.5
0.825	491.5	3.2	-85.5
0.85	494.2	3.3	-89.9
0.875	495.0	3.3	-88.1
0.9	494.7	3.3	-88.8
0.925	493.3	3.3	-89.9
0.95	484.2	3.6	-95.8
0.975	447.3	7.3	-222.4
1	379.9	14.3	-441.7

Table 4: Regression coefficients.

The coefficients a_j are normalized with their maximum values, and are represented as a function of ψ in Fig. A.18.

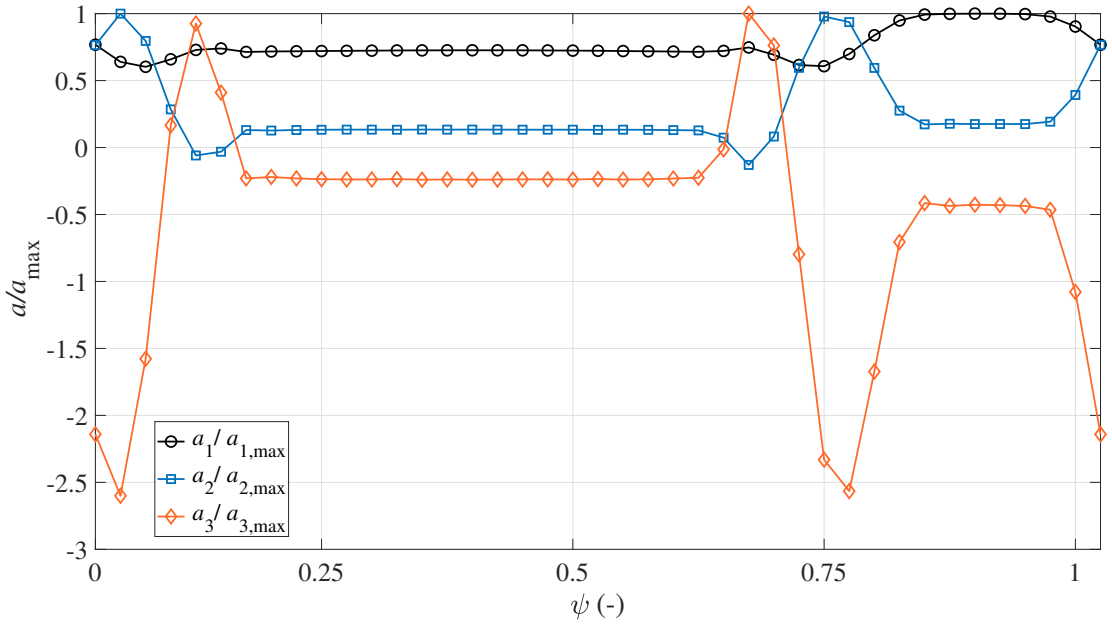

Figure A.18: Regression coefficients normalized with their maximum values in a single meshing cycle.

Appendix B. Damping Implementation

This appendix provides details regarding the damping models used for the dynamic simulation.

Appendix B.1. Minimal damping

The estimate of the minimal damping was obtained on the basis of [32]. In particular, the damping coefficient c_{m} was estimated considering the energy dissipated during the impact of gears as a consequence of the propagation of elastic waves within the material. This phenomenon can not be avoided and this dissipative effect is always present even when all other forms of dissipation are prevented. As a consequence, the dissipation due to the propagation of elastic waves defines the minimum value of damping for the mechanical system.

Given the initial (before the impact) relative speed of the engaging teeth $\dot{q}_0$, the coefficient of dissipation d (reported in Fig. B.19 [32]) was used to calculate the final (after the impact) relative speed $\dot{q}_{\mathrm{f}}$ and the total energy dissipated E_{dis}:

$$\dot{q}_{\mathrm{f}} = (1-d)\dot{q}_0 \tag{B.1}$$

$$E_{\mathrm{dis}} = \frac{I}{4R_{\mathrm{b}}^2}(\dot{q}_0{}^2 - \dot{q}_{\mathrm{f}}{}^2) = \frac{I}{4R_{\mathrm{b}}^2}\dot{q}_0{}^2(2d-d^2) \tag{B.2}$$

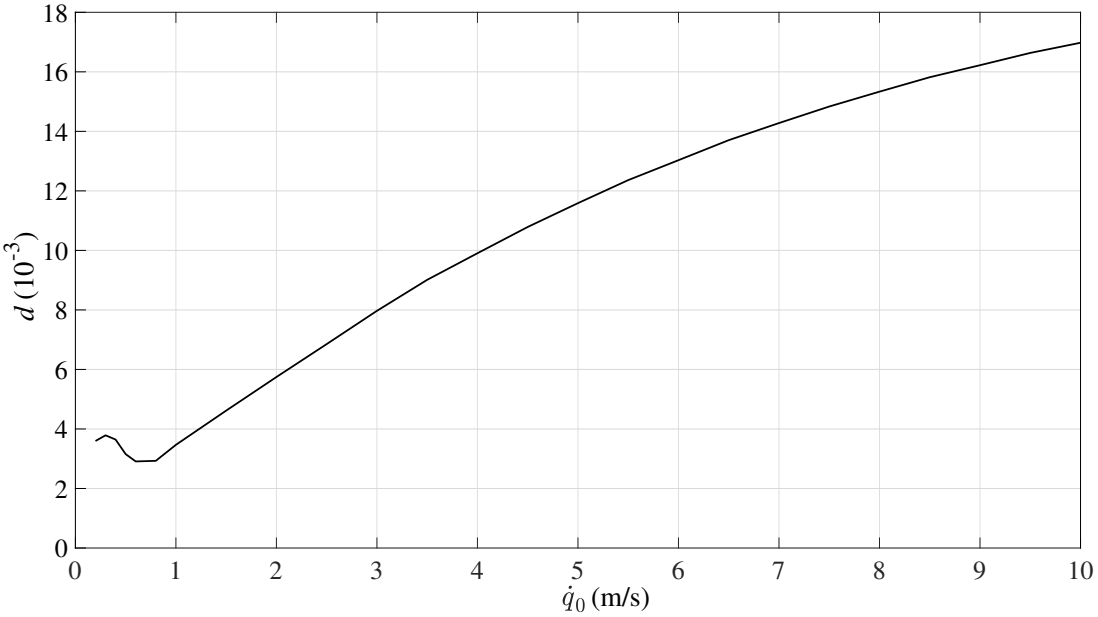

Figure B.19: Coefficient of dissipation as a function of the relative impact speed.

By approximating $\dot{q}(t)$ during the impact with a cosine function of time with amplitude $\dot{q}_0$ and period T equal to the reciprocal of the natural frequency of the system:

$$\dot{q}(t) = \dot{q}_0 \cos(2\pi\frac{t}{T}) \tag{B.3}$$

the total mechanical energy dissipated in the impact can be calculated as:

$$E_{\mathrm{dis}} = \int_0^{T/2} c\dot{q}(t)\dot{q}(t)dt = \int_0^{T/2} c\dot{q}_0{}^2\cos^2(2\pi\frac{t}{T})dt \tag{B.4}$$

Equating equations B.2 and B.4 the damping coefficient c_{m} can be calculated as:

$$c_{\mathrm{m}} = \frac{2E_{\mathrm{dis}}}{(T/2)\dot{q}_0{}^2} = \frac{I}{R_{\mathrm{b}}^2 T}(2d-d^2) \tag{B.5}$$

Appendix B.2. Gerber's semi-empirical damping model

In this approach, the total damping ratio is based on the interpolation of experimental results obtained through gear test rigs. Given the distance between the center of the gears a in mm, the dynamic viscosity of a typical lubricant η in mPas and the tangential speed of the gears v_t in m/s, the following expression is proposed for ζ:

$$\zeta = 2.2 \cdot 10^{-4}(a-23)^{0.55}(\eta+39)^{0.27}(v_t-5)^{0.53} \tag{B.6}$$

The results obtained for the transmission examined in the present paper for which $a = 100.5$ mm, $\eta = 50$ mPas, and $v_t > 5$ m/s, are plotted in Fig. B.20.

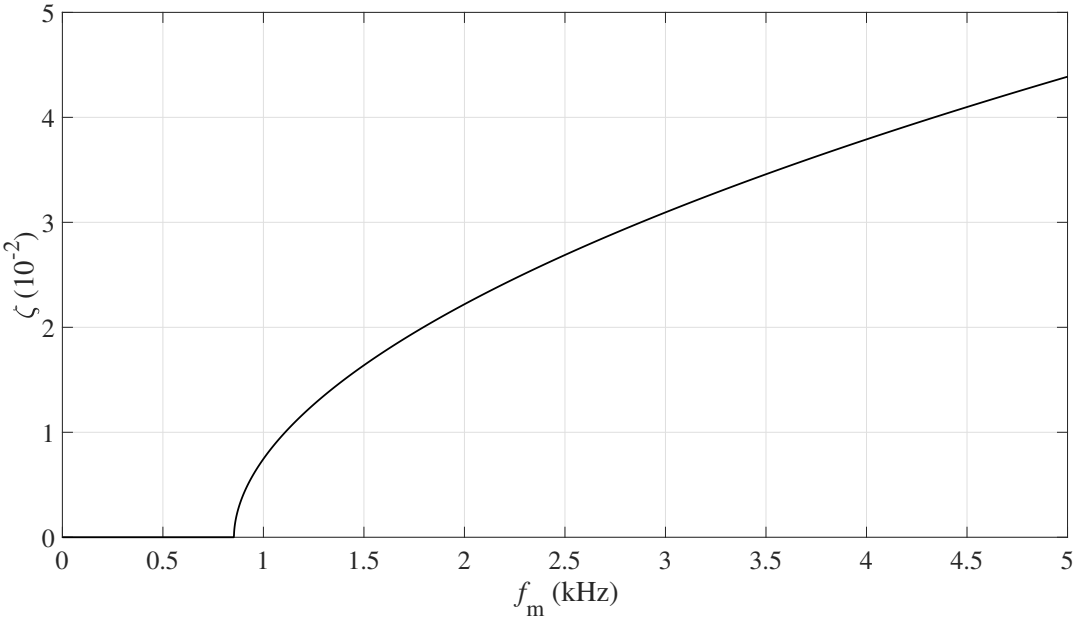

Figure B.20: Gerber's damping ratio as a function of the tangential speed of the gears

At lower tangential speeds ($v_t < 1$ m/s) the order of magnitude of the damping predicted by the two models is the same. The values obtained confirm that the dissipation due to the propagation of elastic waves represents a reasonable underestimation of the dissipative phenomena present in the transmission.

References

[1] H. N. Özgüven, D. Houser, Mathematical models used in gear dynamics—a review, Journal of Sound and Vibration 121 (3) (1988) 383–411. doi:10.1016/s0022-460x(88)80365-1.

[2] G. W. Blankenship, R. Singh, A comparative study of selected gear mesh interface dynamic models, in: 6th International Power Transmission and Gearing Conference: Advancing Power Transmission Into the 21st Century, American Society of Mechanical Engineers, 1992. doi:10.1115/detc1992-0017.

[3] J. Wang, R. Li, , X. Peng, Survey of nonlinear vibration of gear transmission systems, Applied Mechanics Reviews 56 (3) (2003) 309–329. doi:10.1115/1.1555660.

[4] C.-H. Liou, H. H. Lin, F. B. Oswald, D. P. Townsend, Effect of contact ratio on spur gear dynamic load with no tooth profile modifications, Journal of Mechanical Design 118 (3) (1996) 439–443. doi:10.1115/1.2826905.

[5] A. Kahraman, G. W. Blankenship, Effect of involute contact ratio on spur gear dynamics, Journal of Mechanical Design 121 (1) (1999) 112–118. doi:10.1115/1.2829411.

[6] K. Ichimaru, F. Hirano, Dynamic behavior of heavy-loaded spur gears, Journal of Engineering for Industry 96 (2) (1974) 373–381. doi:10.1115/1.3438339.

[7] V. K. Tamminana, A. Kahraman, S. Vijayakar, A study of the relationship between the dynamic factors and the dynamic transmission error of spur gear pairs, Journal of Mechanical Design 129 (1) (2006) 75–84. doi:10.1115/1.2359470.

[8] M. Amabili, A. Rivola, Dynamic analysis of spur gear pairs: steady-state response and stability of the sdof model with time-varying meshing damping, Mechanical Systems and Signal Processing 11 (3) (1997) 375–390. doi:10.1006/mssp.1996.0072.

[9] J. Kuang, A. Lin, Theoretical aspects of torque responses in spur gearing due to mesh stiffness variation, Mechanical Systems and Signal Processing 17 (2) (2003) 255–271. doi:10.1006/mssp.2002.1516.

[10] Y. Cai, T. Hayashi, The linear approximated equation of vibration of a pair of spur gears (theory and experiment), Journal of Mechanical Design 116 (2) (1994) 558–564. doi:10.1115/1.2919414.

[11] A. Kahraman, G. W. Blankenship, Effect of involute tip relief on dynamic response of spur gear pairs, Journal of Mechanical Design 121 (2) (1999) 313–315. doi:10.1115/1.2829460.

[12] T. Eritenel, R. G. Parker, Nonlinear vibration of gears with tooth surface modifications, Journal of Vibration and Acoustics 135 (5). doi:10.1115/1.4023913.

[13] Q. Chen, Y. Wang, W. Tian, Y. Wu, Y. Chen, An improved nonlinear dynamic model of gear pair with tooth surface microscopic features, Nonlinear Dynamics 96 (2) (2019) 1615–1634. doi:10.1007/s11071-019-04874-1.

[14] M. B. Sánchez, M. Pleguezuelos, J. I. Pedrero, Influence of profile modifications on meshing stiffness, load sharing, and trasnsmission error of involute spur gears, Mechanism and Machine Theory 139 (2019) 506–525. doi:10.1016/j.mechmachtheory.2019.05.014.

[15] J. Wang, J. Yang, Y. Lin, Y. He, Analytical investigation of profile shifts on the mesh stiffness and dynamic characteristics of spur gears, Mechanism and Machine Theory 167 (2022) 104529. doi:10.1016/j.mechmachtheory.2021.104529.

[16] S. Theodossiades, S. Natsiavas, Non-linear dynamics of gear-pair systems with periodic stiffness and backlash, Journal of Sound and Vibration 229 (2) (2000) 287–310. doi:10.1006/jsvi.1999.2490.

[17] J. fei Shi, X. feng Gou, L. yun Zhu, Modeling and analysis of a spur gear pair considering multi-state mesh with time-varying parameters and backlash, Mechanism and Machine Theory 134 (2019) 582–603. doi:10.1016/j.mechmachtheory.2019.01.018.

[18] Z. Zhu, L. Cheng, R. Xu, R. Zhu, Impacts of backlash on nonlinear dynamic characteristic of encased differential planetary gear train, Shock and Vibration 2019 (2019) 1–15. doi:10.1155/2019/9347925.

[19] D. Xiang, Y. Shen, Y. Wei, A contact force model considering meshing and collision states for dynamic analysis in helical gear system, Chinese Journal of Mechanical Engineering 32 (1). doi:10.1186/s10033-019-0359-1.

[20] T. Eritenel, R. G. Parker, An investigation of tooth mesh nonlinearity and partial contact loss in gear pairs using a lumped-parameter model, Mechanism and Machine Theory 56 (2012) 28–51. doi:10.1016/j.mechmachtheory.2012.05.002.

[21] E. Sakaridis, V. Spitas, C. Spitas, Non-linear modeling of gear drive dynamics incorporating intermittent tooth contact analysis and tooth eigenvibrations, Mechanism and Machine Theory 136 (2019) 307–333. doi:10.1016/j.mechmachtheory.2019.03.012.

[22] A. Laderou, M. Mohammadpour, S. Theodossiades, R. Daubney, G. Meeks, On the effect of DLC and WCC coatings on the efficiency of manual transmission gear pairs, Applied Sciences 10 (9) (2020) 3102. doi:10.3390/app10093102.

[23] C. Lim, W. Stronge, Oblique elastic–plastic impact between rough cylinders in plane strain, International Journal of Engineering Science 37 (1) (1999) 97–122. doi:10.1016/s0020-7225(98)00026-3.

[24] J. Wang, J. Zhang, Z. Yao, X. Yang, R. Sun, Y. Zhao, Nonlinear characteristics of a multi-degree-of-freedom spur gear system with bending-torsional coupling vibration, Mechanical Systems and Signal Processing 121 (2019) 810–827. doi:10.1016/j.ymssp.2018.12.002.

[25] C. Su, S. Wang, Y. Liu, P. Dong, X. Xu, Coupled vibrations of a drive system during automatic transmission, Advances in Mechanical Engineering 11 (3) (2019) 168781401983350. doi:10.1177/1687814019833508.

[26] T. Eritenel, R. G. Parker, Three-dimensional nonlinear vibration of gear pairs, Journal of Sound and Vibration 331 (15) (2012) 3628–3648. doi:10.1016/j.jsv.2012.03.019.

[27] P. Velex, M. Maatar, A mathematical model for analyzing the influence of shape deviations and mounting errors on gear dynamic behaviour, Journal of Sound and Vibration 191 (5) (1996) 629–660. doi:10.1006/jsvi.1996.0148.

[28] Y. Yang, N. Hu, J. Tang, J. Hu, L. Zhang, Z. Cheng, Dynamic analysis for a spur geared rotor system with tooth tip chipping

based on an improved time-varying mesh stiffness model, Mechanism and Machine Theory 165 (2021) 104435. doi:10.1016/j.mechmachtheory.2021.104435.

[29] C. G. Cooley, C. Liu, X. Dai, R. G. Parker, Gear tooth mesh stiffness: A comparison of calculation approaches, Mechanism and Machine Theory 105 (2016) 540–553. doi:10.1016/j.mechmachtheory.2016.07.021.

[30] X. Dai, C. G. Cooley, R. G. Parker, An efficient hybrid analytical-computational method for nonlinear vibration of spur gear pairs, Journal of Vibration and Acoustics 141 (1). doi:10.1115/1.4040674.

[31] M. A. Hotait, A. Kahraman, Experiments on the relationship between the dynamic transmission error and the dynamic stress factor of spur gear pairs, Mechanism and Machine Theory (2013) 116–128doi:10.1016/j.mechmachtheory.2013.07.006.

[32] M. Abruzzo, M. Beghini, C. Santus, Mechanical energy dissipation due to the propagation of elastic waves during the lateral impact of elastic cylinders, Journal of Sound and Vibration (2022) 117075doi:10.1016/j.jsv.2022.117075.

[33] H. Gerber, Innere dynamische zusatzkräfte bei stirnradgetrieben - modellbildung, innere anregung und dämpfung, Dissertation, Technische Universität München, München (1984).

[34] Y. Benaïcha, J. Perret-Liaudet, J.-D. Beley, E. Rigaud, F. Thouverez, On a flexible multibody modelling approach using FE-based contact formulation for describing gear transmission error, Mechanism and Machine Theory 167 (2022) 104505. doi:10.1016/j.mechmachtheory.2021.104505.

[35] M. Beghini, F. Presicce, C. Santus, A method to define profile modification of spur gear and minimize thetransmission error, Proceedings of AGMA Fall Technical Meeting, Milwakee.

[36] M. Beghini, F. Presicce, C. Santus, Proposal for tip relief modification to reduce noise in spur gears andsensitivity to meshing conditions, VDI Conference 2005, Monaco.

[37] C. Natali, M. Battarra, G. Dalpiaz, E. Mucchi, A critical review on FE-based methods for mesh stiffness estimation in spur gears, Mechanism and Machine Theory 161 (2021) 104319. doi:10.1016/j.mechmachtheory.2021.104319.

[38] M. Abruzzo, M. Beghini, C. Santus, S. Manconi, Dynamic behavior of a power re-circulating gear test rig including periodic variation of mesh stiffness and static transmission error, Mechanism and Machine Theory 159 (2021) 104247. doi:10.1016/j.mechmachtheory.2021.104247.

[39] L. F. Shampine, M. W. Reichelt, The MATLAB ODE suite, SIAM Journal on Scientific Computing 18 (1) (1997) 1–22. doi:10.1137/s1064827594276424.